Nanofiltration thin film composite membrane on either the internal or the external surface of a polysulfone hollow fiber

Carlos Echaide-Górriz, Magdalena Malankowska, Carlos Téllez, Joaquín Coronas*

Chemical and Environmental Engineering Department, Instituto de Nanociencia de Aragón (INA) and Instituto de Ciencia de Materiales de Aragón (ICMA), Universidad de Zaragoza-CSIC, 50018 Zaragoza, Spain

*Corresponding author: coronas@unizar.es

Abstract

The inner and outer surfaces of a porous hollow fiber polysulfone support are compared as substrates for the synthesis of polyamide thin film composite (TFC) membranes by interfacial polymerization. While both surfaces have pores common of microfiltration membranes, the inner surface has a larger pore diameter than the outer surface (2700 nm compared to 950 nm). The inner TFC membrane showed higher water nanofiltration permeance than the outer (2.20±0.17 compared to 0.13±0.03 $L \cdot m^{-2} \cdot h^{-1} \cdot bar^{-1}$). This was due to the influence of the porosity and roughness which were different on both support surfaces. These membranes are interesting because they were synthesized in a hollow fiber support with a high membrane area per volume unit (ca. 6900 m^2/m^3) and the substrate used was commercial, which means that the TFC membrane obtained is suitable for industrial application. A mathematical simulation of the nanofiltration run with COMSOL Multiphysics 5.3 software confirmed the experimental trends observed.

Keywords

Interfacial polymerization; Thin film composite; Hollow fiber; Microfluidics; Nanofiltration

Introduction

Nanofiltration is a process for an efficient and economical separation of different mixtures that involve water and organic solvents. Various membranes with different structures have been studied and synthesized for this purpose, thin film composite membranes (TFC) being especially noteworthy. The structure of these membranes, which consist of an asymmetric support with a selective thin layer on top, enables the chemistry and porosity of both layers of the composite to be changed separately.[1] For this reason, many combinations of polymers have been reported,[2] some of them being commercial membranes but others tailor made.

Jeong et al. synthesized a thin film nanocomposite membrane (TFN) including zeolites as fillers with the goal of enhancing the permeability of the membrane in nanofiltration while maintaining high rejection values.[3] Thereafter, other nanostructures were used to modify TFC membranes giving rise to new TFN membranes such as, hollow zeolite spheres,[4] functionalized TiO_2,[5] functionalized multiwalled carbon nanotubes,[6] UZM-5,[7] and MOF nanoparticles.[8] However, all these investigations were carried out on flat sheet support membranes. Other authors have studied the interfacial polymerization method for TFC synthesis on hollow fiber and tubular membrane supports. Here, two possibilities arise: the creation of the thin film on the shell side of the corresponding tube and the synthesis on its lumen side. Parthasarathy et al.[9] synthesized for the first time a PA thin film on the outer surface of a hollow fiber, and Verissimo et al.[10] did the same on the lumen side (polyetherimide, PEI) some years later. These investigations were continued by other researchers that observed the effect on the membrane performance of different hollow fiber substrate materials such as PVC, polysulfone and PES among others.[11–13] These authors continued looking into TFC membranes, developing composite membranes with a hyperbranched polymer as the thin film.[14,15]

The interest in studying the behaviour of hollow fiber membranes lies in the fact that they not only open the door to membrane modules for process intensification in terms of high m^2/m^3 ratio, and therefore to high efficiency and favourable economy, but also to microfluidic synthesis. Among all the strategies studied so far in the field, microfluidic synthesis in particular leads to the reduction in the usage of reactants and to synthesis optimization.[16,17] This technique is only considered when the Reynolds and the thermal Péclet numbers are below 250 (strict laminar flow) and 1000 (higher diffusion contribution over convection), respectively.[17] These conditions, which can give a precise control of the synthesis parameters, would only take place in hollow fibers with an inner diameter less than 500 μm.[17] This is of great interest in the

interfacial polymerization procedure for the TFC membranes fabrication because of its sequential nature, since it would be interesting to see what effect a continuous laminar flow can have in this method of synthesis.

There are few publications about the impact of a hollow fiber substrate structure on the formation of the PA thin film in a TFC membrane.[11,18] However, these studies are generally focused on low pore size substrates used in membrane ultrafiltration, while in the present work a microfiltration substrate is used, which is rarely applied in TFC fabrication. Besides, the influence of the substrate on the PA thin film formation has been intensively studied in flat conformations rather than in hollow fibers. For instance, Ghosh and Hoek[19] studied the impact of the support structure and chemistry on the TFC membrane. Jimenez-Solomon et al.[20] observed the influence of the hydrophilicity or hydrophobicity and the roughness on the final TFC membrane. Lee et al.[21] recently studied the formation of highly porous microstructured supports, where the proportion of polymer in the casting solution used in the phase inversion was reduced. This study was amplified to the influence of pore size and porosity on the formation of a highly permeable PA layer of a TFC membrane. Once more, this work was only focused on flat membranes. For this reason, a study of these effects in hollow fiber membranes is of considerable interest because it would contribute to the optimization of the synthesis and the maximization of the solvent permeance.

The present study examines the effect of roughness in a hollow fiber where a thin PA film was synthesized separately on either the outer surface or the inner surface for nanofiltration applications (filtrating always from the PA side: in-out in the inner TFC and out-in in the outer TFC configuration). Generally, ultrafiltration substrates have been used to fabricate TFC membranes,[19,22,23] but in the current work a commercial microfiltration polysulfone support provided by the membrane manufacturer Polymem was used instead. Since the membrane was designed to separate from the outer surface, the manufacture states that the pore size there should be above 200 nm. This was confirmed by our characterization. The goal of the study is to characterize both surfaces of the hollow fiber support and to synthesize PA thin films on the surfaces by interfacial polymerization. It is worth mentioning that the previous studies by Verissimo et al. and Kong et al. were carried out on PEI and PVC fibers, with external and internal diameters of 1.06 mm and 0.74 mm, and 1.16 mm and 0.78 mm, respectively.[10,11] In this work, not only a different polymer was used (polysulfone) but also narrower external and internal diameters than in both of the previous studies were applied (0.38 mm and 0.25 mm, respectively). This increases the process intensification in terms of volumetric area and the complexity of membrane fabrication due to the more intricate access to the hollow

fiber lumen. The separation application was focused on the removal of Acridine Orange (AO, 260 Da) from water. The experimental procedure was adapted for the inner and outer syntheses: when the PA was formed on the outer surface, the synthesis was carried out by the usual interfacial polymerization method,[8,23,24] whereas when the PA was formed on the inner surface the interfacial polymerization was carried out by microfluidics. The influence of the support pore size and roughness, as well as the interfacial synthesis procedure, on the final TFC membrane is evaluated. Finally, a mathematical simulation was carried out with COMSOL Multiphysics 5.3 software and the performances of the membranes were compared to others reported in the literature.

Experimental

Hollow fiber supports

The polysulfone hollow fiber supports where kindly supplied by the membrane manufacturer Polymem. These hollow fibers were designed for microfiltration processes, with theoretical pore sizes of 200 nm, and inner and outer diameters of 250 and 380 μm, respectively.

PA layer synthesis on the outer layer

The hollow fiber substrates were firstly immersed in a solution of 2% (w/v) MPD (m-phenilenediamine - 99 %, Sigma Aldrich) in deionized water for 2 min, and the excess solution was removed using tissue paper. The hollow fiber supports were then immersed in a solution of 0.1 (w/v) TMC (trymesoil chloride – 98%, Sigma Aldrich) in n-hexane (extra pure, Scharlab) for 1 min. The last two steps consisted of washing out the remains of both solutions with n-hexane first and deionized water afterwards. Once the TFC membrane was fabricated it was sealed with Araldite® epoxy resin in a stainless steel membrane module designed for this application: the feed solution flows through the shell side, while the permeate flows through one of the two ends of the lumen side of the membrane. The other end is deliberately clogged (see Fig. S1A).

*Table 1. TFC synthesis parameters. *Contact time between the membrane and the chemical indicated*

	MPD (% w/v)	**Time MPD* (min)**	**Excess removal**	**TMC (% w/v)**	**Time TMC* (min)**
Outer TFC	2	2	Drying with tissue paper	0.1	1

Inner TFC	2	5	Washing out with cyclohexane	0.3	1.5

PA layer synthesis on the inner layer

The synthesis of the PA thin film on the inner surface of the hollow fiber support was carried out following the method reported by Verissimo et al.[10] for a single fiber, although parameters such as the hollow fiber diameters (0.25 mm inner diameter instead of 0.74 mm), concentrations and contact times are different in the synthesis presented here. As Chai and Krantz observed,[25] the reaction between the monomers MPD and TMC is very fast since only a few seconds are needed to form the aromatic PA. Therefore, a residence time of 7 s was chosen for the TMC solution, although it is known that the global reaction rate progressively decreases with time, due to the mass transfer resistance created by the growing PA film. In these conditions, the MPD solution, whose composition was identical to that used in the previous synthesis (2% w/v), was fed at a rate of 70 µL/min for 5 min. Pure cyclohexane (Scharlab, extra pure) was then pumped at a rate of 157 µL/min for 1 min (reducing in this case the residence time to 3 s) to remove the excess solution from the lumen side. A solution of 0.3 % (w/v) of TMC in n-hexane was then pumped at a rate of 70 µL/min to start the interfacial synthesis of the PA. All these fluxes correspond to a single fiber. The lumen side was washed first with n-hexane and next with deionized water. The fabricated TFC membrane was then placed in a membrane module, sealing both extremes with Araldite®, as shown in Fig. S1B.

Characterization

A FEI-Inspect F20 scanning electron microscope (SEM) was used at an acceleration voltage between 10 and 20 kV with spots between 2.5 and 3.5 nm to study some selected membrane samples. Three randomly selected areas of each of the outer and inner sides of the hollow fiber support were examined by SEM. Both the morphology and pore size distribution over the surface were observed. The pore sizes were measured with ImageJ® software and the values were then averaged. The outer and inner surfaces of the TFC membranes were also observed by SEM microscopy, but only one single area of each. The cross section areas of both the bare support and TFC membranes were also explored.

Atomic force microscopy (AFM) was used to measure the roughness on both the outer and inner surfaces of the hollow fiber supports. Three different areas of 10x10 µm in size were observed on the outer surface of the substrate, and the roughness value was measured and averaged. On the inner surface, in contrast, three areas of different dimensions were observed: 30x30 µm, 10x10 µm and 4x4 µm, and the same

statistical treatment was applied to the roughness values obtained. Besides, a measurement of the pore size distribution in the membrane was obtained in several areas of both surfaces. The equipment used was a VEECO Multimode 8 with a tapping mode used in ambient air conditions together with a single crystal silicon antimony doped cantilever provided by NT-MDT Spectrum Instruments.

Transmission electron microscopy (TEM) was used to observe microtome samples of the TFC membranes. The samples were prepared by cutting segments of both types of the fabricated TFC membranes, with the PA on the inner and outer surfaces of the hollow fiber, and embedding them in epoxy resin. These pieces of resin were then cut on a Leica EM UC7 ultramicrotome and deposited on copper grids. A FEI Tecnai T20 transmission electron microscope was used at an acceleration voltage of 30 kV.

XPS experiments were conducted to quantify the quantity of carbon (C), oxygen (O) and nitrogen (N) at different depth while etching the polyamide thin layer. The ratios C/N and O/N give an estimation of the overall cross-linking degree in the polymer, when they are compared.[26] XPS characterization was performed with a Kratos Axis Ultra spectrometer employing a monochromatic Al Ka (1486.6 eV) X-ray source at 10 mA and 15 kV and a power of 150 W. The samples were first evacuated at room temperature (pressures near 1011 bar were observed during surface analysis) and analyzed in 0.11 x 0.11 mm^2 areas under the same conditions.

Mathematical model

In order to compare with the experimental results and understand the working principle of the fabricated membranes, the mathematical simulation was performed. The fluid dynamics modelling was carried out in COMSOL Multiphysics 5.3 software. It is one of the most inclusive softwares used for the CFD (computational fluid dynamics) computation due to its wide range of applications, relatively straightforward user interface and possibility to customize the model.

Laminar flow physics was used to describe the flow across the hollow fiber. The momentum conservation for laminar flow of incompressible fluids (Equation 1) together with the mass conservation (Equation 2), i.e. Navier-Stokes equation, were solved:

$$\rho(\mathbf{u}\cdot\nabla)\mathbf{u} = \nabla\cdot\left[-p\mathbf{I} + \mu(\nabla\mathbf{u} + (\nabla\mathbf{u})^T) - \frac{2}{3}\mu(\nabla\cdot\mathbf{u})\mathbf{I}\right] + F \qquad \text{(Equation 1)}$$

$$\nabla\cdot(\rho\mathbf{u}) = 0 \qquad \text{(Equation 2)}$$

where, ρ is the liquid density, **u** stands for the flow velocity vector field, p is the pressure, μ is the liquid viscosity, superscript T is transposed of a matrix and F is a source term.

In Equation 1, the terms on the left side are the acceleration forces, and on the right hand side, there are pressure gradient and viscous forces. Following assumptions have been made:

- No back-flow permitted.
- No slip conditions on the walls, **u** = 0.
- The outlet pressure was set as the atmospheric value.

In addition to the velocity profile solving, the mass balance and transport equation was used from a standard convection-diffusion mass transfer expression that under steady state becomes (Equation 3):

$$\mathbf{u} \cdot \nabla c_i = D \cdot \nabla^2 c_i \qquad \text{(Equation 3)}$$

where, c is the concentration of species and D is the diffusion coefficient.

Nanofiltration

The modules prepared contained only one fiber each. Therefore, the inner and outer diameters of the hollow fibers were 250 and 380 μm, respectively. The modules prepared, of 8 cm as effective length, had effective surfaces of $3.0 \cdot 10^{-5}$ m^2 in case of the filtration from the lumen to the shell side and $4.7 \cdot 10^{-5}$ m^2 in case of the filtration in the other way around.

Firstly, the bare hollow fiber supports were measured in nanofiltration at a feed pressure of 4 bar, 200 μL/min of feed flux and a temperature of 20 ºC. The feed composition was 15 mg/L of Acridine Orange (AO, 260 Da – 55% dye content, Across Organics) in deionized water. The performances of the supports were observed by filtrating separately from the outer or inner surfaces.

The measurements of the fabricated TFC membranes were carried out under the same conditions, except for the pressure, which in this case was 8 bar. Both types of membranes, with the PA synthesized on the outer or inner surfaces, were tested in the AO nanofiltration. In the case of the membranes with the PA layer on the outer surface, the AO solution was fed from the shell side, and in the case of the membranes with the PA layer on the inner surface, the feed was pumped from the lumen side.

The experiments were performed in the experimental system that is schematically presented in Fig. 1. The membranes were placed in the module (see Fig S1 to see two different membrane modules used depending on whether the permeation is out-in or in-out), pressure valve, two manometers (at the feed and retentate side) and a thermocouple to control the temperature. The installation consisted as well of a tank at

atmospheric pressure that contained the feed solution, a pump and two branches. One of them is the by-pass, formed by a single valve that regulates the flow towards the tank. The other one is the branch with the membrane module.

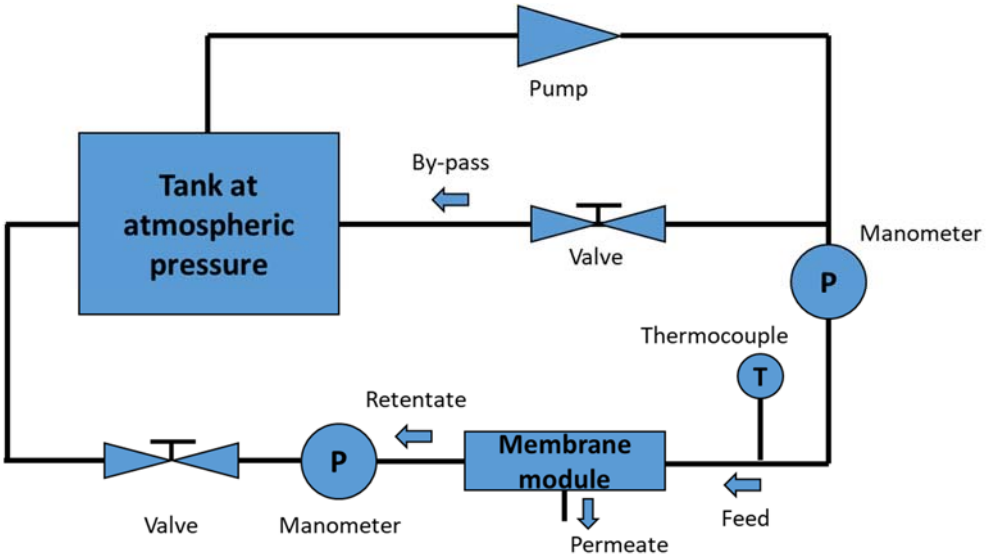

Fig. 1. Installation for the nanofiltration tests.

In all cases, the membrane performances were characterized by measuring the permeances of water through them (equation 4), and analyzing the solute concentration in both retentate and permeate to calculate the rejection (equation 5). A Jasco V-670 UV-Vis spectrophotometer was used to obtain the AO concentration at 291 nm as wavelengths of maximum absorbance.

$$Permeance = \frac{Q}{\Delta P} = \frac{V}{A \cdot t \cdot \Delta P} \quad \text{(Equation 4)}$$

$$Rejection\ (\%) = \left(1 - \frac{C_{permeate}}{C_{feed}}\right) \cdot 100 \quad \text{(Equation 5)}$$

Results and discussion

Characterization

The SEM imaging reveals a slightly asymmetric distribution of the porosity across the bare hollow fibers cross section. As observed in Fig. 2A, the pore size seems to increase from the outer surface (Fig. 2B) to the inner surface (Fig. 2C). This progressive radial densification along the cross section is consistent with the fact that this membrane was originally designed to separate water from solid suspensions in microfiltration from the outer surface.

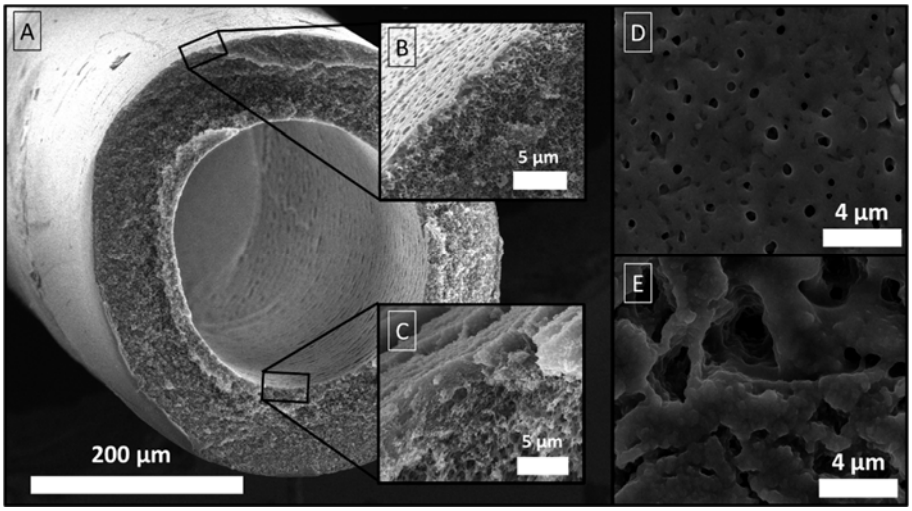

Fig. 2. Cross section area of the fresh hollow fiber (A), with insets of the cross section areas closer to the outer and inner surfaces (B and C, respectively). SEM images of the outer (D) and inner (E) surfaces of the bare hollow fiber.

This observation was also confirmed by the SEM images taken from both the outer and inner surfaces of the bare polysulfone hollow fibers. The outer surface seems to be smoother and shows a homogeneous distribution of the superficial porosity (Fig. 2D). In contrast, the inner surface is rougher and has a heterogeneous porosity, with wider pores in average than the outer surface (see Fig. 2E).

As it can be seen in the SEM images, there are obvious differences in the porosities of both surfaces. This was confirmed by the pore size calculations: while on the inner surface there are pore apertures of 2700 ± 1200 nm in diameter, on the outer surface the apertures are of 950 ± 260 nm (see Table 2). These values evidence the wide distribution of pores on the inner surface, where the standard deviation calculated was

around 50% of the average value. In contrast, the outer surface shows a narrower deviation range together with a lower average value.

Table 2. RMS (root mean square) roughness (calculated with the AFM software) and pore sizes (calculated using the ImageJ® software on the SEM images of three different areas of both surfaces of the hollow fiber) of both inner and outer surfaces

	RMS roughness (nm)	Pore size (nm)
Inner	1000 ± 660	2700 ± 1200
Outer	270 ± 50	950 ± 260

The AFM microscopy corroborated the differences in morphology of both the outer and inner surfaces of the polysulfone supports (see Fig. 3A and 3B, respectively). The superficial pores on the outer surface seem homogeneously distributed, with a relatively narrow range of pore diameters. In contrast, the inner surface has a rather heterogeneous distribution of pore sizes and in turn higher pore diameters. The roughness of both surfaces are clearly different. The outer surface is smoother than the inner surface: in average, the RMS values are lower on the outer side than on the inner side (270 ± 50 nm compared to 1000 ± 660 nm, see Table 2), although the standard deviation is smaller on the inner than on the outer surface. This gives an idea of the irregularity of the inner surface, compared to the homogeneousness of the outer. This will have a decisive importance in the membranes preparation, as will be shown below.

There are no significant differences in the morphology between the SEM images taken from the inner and outer surfaces of the fabricated TFC membranes (see Fig. S2A and S2B). Only the typical ring-like shapes of the PA film were observed together with the suggestion of an ultrathin film of PA coating the polysulfone support. This is consistent with the findings of several publications in the field.[8,23,24,26] However, there are differences below the PA films, as can be seen in Figs. 3C and 3D which show the cross section view of the outer and inner coatings deposited on the polysulfone supports. The narrow pores seen in the AFM images of the outer surface of the bare hollow fibers (see Fig. 3A) were covered by the PA film (see Fig. 3C). The same seems to have occurred on the inner surface, whose large pores seen in Fig. 3B were totally covered by the PA thin film even in the absence of full contact between the PA and polysulfone surfaces, leaving hollow spaces below (see Fig. 3D). TEM images of both types of microtomed samples show some

differences in the PA film consistency, probably generated by the different inner/outer porosity discussed above. The PA thin film synthesized on the outer, smoother surface of the hollow fiber support appears directly attached to the polysulfone surface and has a similar morphology and thickness as the PA thin films shown in the previous publications of Ghosh and Hoek[19] and Jeong et al.[3] (70 ± 13 nm, see Fig. 3E). In contrast, the PA thin film formed on the inner surface, being thin in agreement with the SEM observations (see Fig. 3D), appears ca. 1 μm above the polysulfone surface (see Fig. 3F). This can be explained by the sample manipulation during the microtome preparation, which may have changed the thin layer orientation. The much larger pores of the inner side of the support allowed the penetration of the resin during the TEM sample preparation, and this resin (as bright in the TEM images as the PA layer) was intercalated between the polysulfone and the PA. All in all, the thickness could be estimated from the SEM image of Fig. 3D, obtaining a result of 51 ± 14 nm, slightly thinner than the outer PA layer in average (see Fig. 3D and 3E for comparison).

In summary, the PA ultrathin layers have about the same thickness when prepared either on the outer or on the inner side of the hollow fiber support, as observed in the SEM and TEM images. Even though the inner PA layer was estimated to be slightly thinner than the outer, it is difficult to conclude it was in fact thinner, since both estimations cannot be necessarily comparable, as they were obtained by different techniques.[27] Considering the PA-polysulfone ensemble, the morphology of the outer surface seems similar to that of the ultrafiltration supports described in the majority of publications relating to nanofiltration and reverse osmosis.[3,8,20,23,24,26] The morphology of the inner surface, though, clearly reveals larger porosity (evidenced as hollow spaces below the continuous PA film) similar to the microfiltration supports recently used by Lee et al.[21] to make highly permeable TFC membranes.

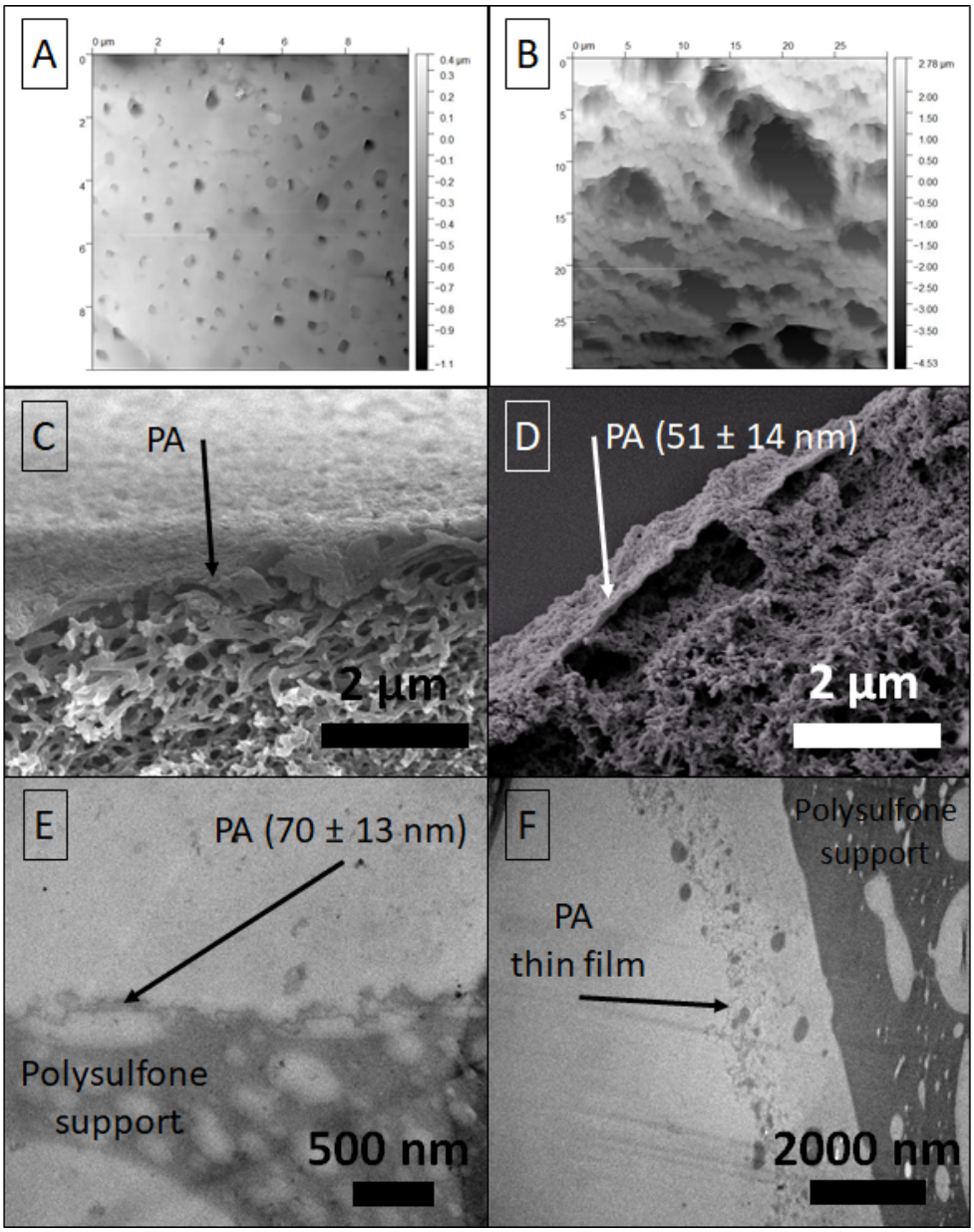

Fig. 3. 2D images of AFM microscopy of the outer surface (A) and the inner surface (B) of the polysulfone hollow fiber support. SEM image of the cross section area of a TFC membrane where the PA was synthesized on the outer surface (C). SEM image of the cross section area of a TFC membrane where the PA was synthesized on the inner surface. As can be seen, even if the substrate is totally covered by the PA thin film, there is not full contact between the PA and polysulfone surfaces. As it is seen, the estimated PA layer thickness is 51 ± 14 nm, based on the measurements taken on the figure itself with the ImageJ® software (D). TEM images of TFC membrane microtomes: outer PA thin film on the outer (E) and PA thin film on the inner (F) surface. In the (E) figure, the PA layer thickness was estimated to be 70 ± 13 nm based on the measurements taken with the ImageJ® software on the figure itself.

Nanofiltration

Hollow fiber substrate performance

The nanofiltration of AO water solutions from each surface, outer and inner, of the hollow fiber support showed the same evolution with time (see Fig.4A). A combination of membrane compression and a fouling phenomenon made the membrane less permeable over time:[2] from 1821 ± 442 and 3820 ± 2785 $L \cdot m^{-2} \cdot h^{-1} \cdot bar^{-1}$ at the first hour to 84 ± 83 and 111 ± 39 $L \cdot m^{-2} \cdot h^{-1} \cdot bar^{-1}$ at the sixth hour from the outer and inner surfaces, respectively. However, the standard deviation remained very high, as shown in the blue columns, from the second hour to the sixth hour (see Fig. 4A). This may come partly from fouling, or even concentration polarization phenomena due to the strong interactions AO – Psf evidenced by the Hansen Solubility Parameter (HSP[28]) Ra of 5.5 $MPa^{1/2}$, lower than 7 $MPa^{1/2}$. This indicates an interaction between both components (calculated as in a previous publication;[23] HSP of AO taken from ref.[23] and HSP of PSf taken from ref.[29]). In fact, Echaide-Górriz et al.[23] previously addressed the fouling effect of AO in TFC membranes. Additionally, the heterogeneity of pore size and roughness in both inner and outer surface also influenced in obtaining such high deviation values. One of the samples exhibited permeances as high as the red columns, but the other sample showed considerably lower values. This can be explained by a widely dispersed pore size distribution on the outer surface, evidenced in the characterization by SEM and AFM (see Table 2), which would have made both samples behave differently in terms of water permeance.

However, on average, the permeance values seem to be higher when filtrating from the inner surface than from the outer. According to Ghosh and Hoek,[19] several surface parameters influence the performance of membrane supports. Pore radius, pore structure, capillary pressure and surface roughness directly influence water permeance. The direct dependence of water permeance on pore radius and roughness, as observed in their experiments,[19] was due to the hollow spaces created by the pores and the wider available surface resulting from the high degree of roughness.[30] These two factors explain the higher water permeance from the shell side than from the lumen in the current experiment since, as shown in Table 2, both pore diameter and roughness are greater on the shell side. In contrast, the water permeance had an inverse dependence on the capillary pressure, which means that the lower the capillary pressure, the higher the water permeance. The Young-Laplace equation describes the relation between the capillary pressure (ΔP) and the cylindrical pore radius of the meniscus (R) as an inverse dependence (see Equation 6, where γ is the surface tension).

$$\Delta P = \frac{2 \cdot \gamma}{R} \qquad \text{(Equation 6)}$$

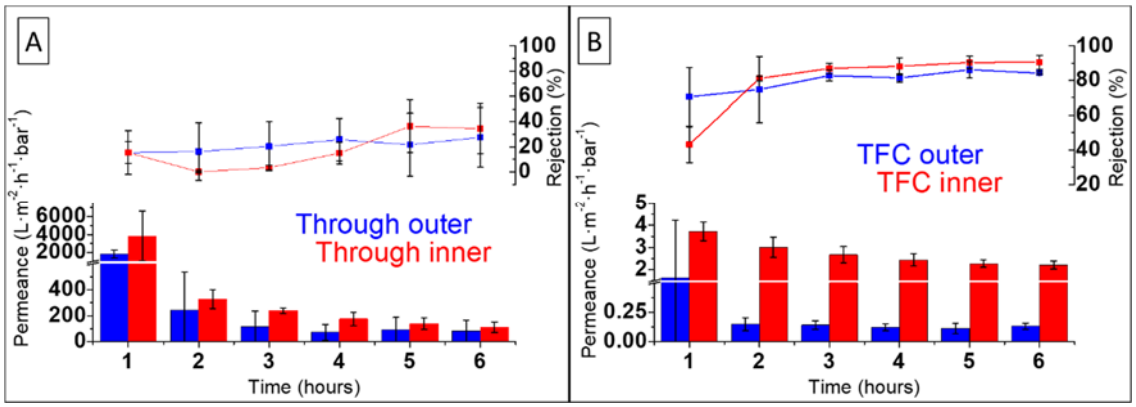

Fig. 4. Nanofiltration performance of the hollow fiber substrates, filtrating from the outer surface to the inner (blue) and from the inner to the outer (red). Two different membrane substrate samples were measured for each case at 4 bar and 20 ^{O}C (A). Nanofiltration performance of the TFC membranes, filtrating from the outer surface to the inner (blue) and from the inner to the outer (red). Three samples were measured at 8 bar and 20 ^{O}C and averaged allowing standard deviation calculations for each case (B).

In the literature, the relation between surface hydrophilicity in membranes and water filtration has been extensively studied.[8,20,23] For instance, Ghosh and Hoek[19] analysed this relation comparing polysulfone supports with different pore sizes, roughness and additives in their porosities (polyethylene glycol (PEG) and/or polyvinyl pyrrolidone). However, they observed that the hydrophilicity did not really have as relevant influence on the water permeance as the other parameters mentioned in the paragraphs above (i.e. roughness and pore size). For this reason, contact angle measurements were not included in this research.

TFC membrane performance

The performances of both TFC membranes, with the PA on the outer or on the inner hollow fiber surface, were considerably different (see Fig. 4B). When the PA was synthesized by microfluidics on the inner surface, the water permeance was much higher than when the PA was synthesized on the outer surface by the conventional methodology: at the sixth hour (steady-state regime), 2.20 ± 0.17 and 0.13 ± 0.03 $L \cdot m^{-2} \cdot h^{-1} \cdot bar^{-1}$ for the inner and outer TFC membranes, respectively. In addition, significant differences were observed in the rejection values at the sixth hour: 90.6 ± 4.0 and 84.3 ± 0.8 % for the inner and outer TFC membranes, respectively. In Fig. 4B it is observed that at the first hour, both inner and outer TFC membranes had poor performances of relatively high water permeances and AO rejections around 40-60% with high deviations. In our view, this phenomenon would be related to a transitionary regime where a mixture of fouling and compression effects phenomena on the thin film may occur. It is observed, in fact, that after one hour, the water permeance starts to stabilize and therefore, the AO rejections tend to increase. This difference in the performance of both types of membranes, favoring those prepared on the inner side of the hollow fiber support, might be explained by a combination of several factors: porosity, pore size and roughness of both surfaces, the PA synthesis method and the substrate hydrophilicity. In the bare polysulfone substrates, the effect of hydrophilicity need not to be considered in line with related publications, where there was no relevant difference in the contact angle values between surfaces of different roughness and pore size values.[19]

To understand the role of the pore size on the interfacial polymerization, it is important to check first the previous investigations of Ghosh and Hoek[19] and Jimenez-Solomon et al.[20] They observed an important effect of the presence of additives such as PEG on the superficial porosities of the substrates and on the creation of the PA thin film by interfacial polymerization. In fact, the consequences of the interactions between PEG in pores and the aqueous solution (MPD in water solution) is quite similar, in our view, to the consequences of the capillary pressure created by the superficial pores of the support. Ghosh and Hoek[19] and Jimenez-Solomon et al.[20] observed that PEG impregnation enhanced the surface hydrophilicity. However, they explained the PEG influence in terms of hydrogen-bonding interactions between PEG and MPD molecules, which tended to slow down the MPD diffusion through the pores until finally reacting with TMC in the water-hexane interface. Nevertheless, the presence of PEG molecules seems to have had contradictory consequences in the two studies. Ghosh and Hoek[19] concluded that the slower diffusion of MPD before reacting with the TMC led to a thinner PA film with a lower solvent permeance but a higher

solute rejection. In contrast, Jimenez-Solomon et al.[20] observed that the presence of PEG gave rise to a thinner thin film with a higher solvent permeance. In any event, both came to the same conclusion about the consequences in terms of the thickness of the PA film, but they did not observe the same effect of the PEG presence on the TFC membrane performance. All in all, rather than being an effect of hydrophilicity, it seems to be the effect of the MPD diffusion during the formation of the membrane which can alter the final PA morphology.

The pore size would affect the capillary pressure, as indicated by the equation of Young-Laplace (Equation 6), which in turn would influence the aqueous solution (MPD in water) diffusion back to the surface prior to the interfacial polymerization. Thus, the capillary pressure of the relatively low size pores found on the outer surface of the bare hollow fiber might have slowed down the MPD diffusion in the formation of the PA thin film, leading to a thinner but denser film with high flow resistance. This was, in fact, the effect of the presence of PEG that was mentioned to create in the previous study of Ghosh and Hoek.[19] However, the PA thin film on the lumen side might have been created with higher MPD diffusion resistances, leading to a more porous PA layer. The capillary pressure in pores can reduce the diffusion resistance of the aqueous solution when MPD is reacting with the TMC from the organic phase, similarly to the presence of PEG (and its interaction with the aqueous solution) in the publications above discussed.[19,20]

The pore sizes corresponding to both sides of the hollow fiber support would also have an additional influence on the performances of the TFC membranes obtained here. In the nanofiltration process, the PA layer isolates the polysulfone porosity from the feed solution, since the first completely covers the polysulfone support (see Fig. S2A and S2B from the SI). When filtrating with a bare polysulfone support, this porosity would be fouled with adsorbed AO molecules (see Fig. 5A), as occurred in Fig. 4A. In contrast, when filtrating with a TFC membrane, the PA coating would protect the support porosity against such fouling (see Fig. 5B). In this way, the part of the support close to the PA film would now have empty pores (due to the lack of full PA-polysulfone contact, as seen above) through which the water molecules can freely flow, enhancing its permeance (see Fig. 4B). Although the outer surface of the support, has smaller pores producing full PA-polysulfone contact and thus a denser composite membrane to the point that the PA would not enhance the water permeance that much. In other words, the smaller pores on the outer surface would be more suitable for fouling with dye than the larger pores on the inner surface.

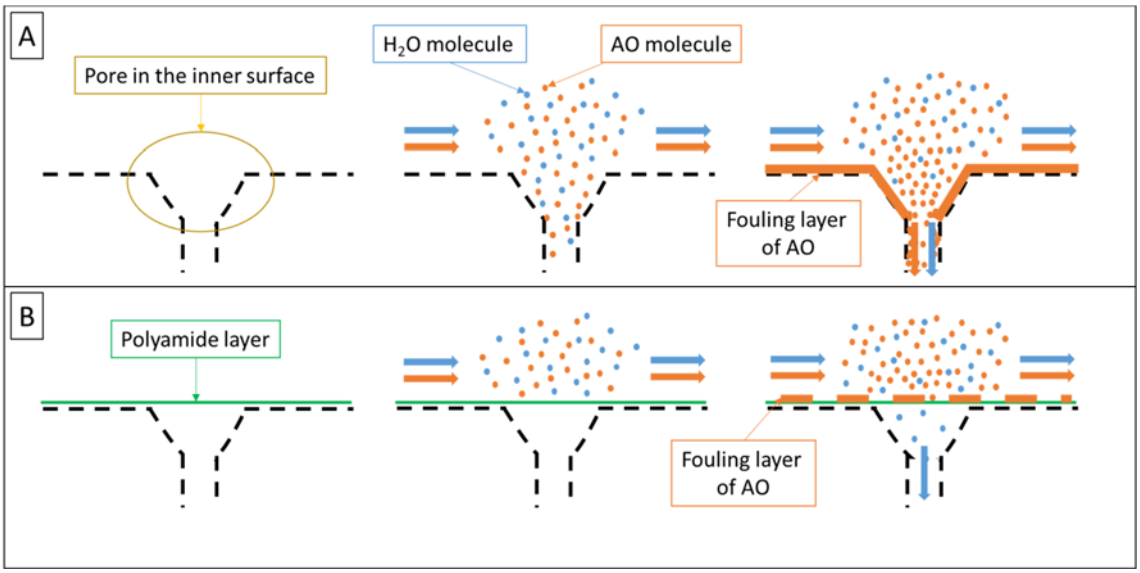

Fig. 5. Scheme of the fouling phenomenon when filtrating with only the bare polysulfone support (A). The same phenomenon, but with the PA layer (the green line) that isolates the support pore from the AO molecules. The pore size and shape were inspired in the pore seen in Fig. 3D, even though there is not a proportional relation between molecules size and pore size in order to give a clear view of the phenomenon explained.

The roughness on both surfaces probably had a considerable influence, as well. Jimenez-Solomon et al.[20] observed that roughness influenced the TFC membranes that they fabricated and measured. Besides, they mentioned that roughness could enhance the anchoring of the PA thin film to the substrate, giving the membrane more stability, even though high roughness could enhance the creation of defects in the thin film. In case of the substrate used in this work, the distinction between roughness and pore size is not that easy, especially, in the inner surface. As seen in Fig. 3D, the big pores do not necessarily enhance the creation of defects during the PA synthesis, since they are used as mere reservoirs for the amine solution, so that the layer is just created on top of them. However, in the outer surface, the interpretation is different, since the surface seems to have more similar pore size and roughness values to the most typical surfaces for TFC synthesis (ultrafiltration substrates with narrower pores and smoother surfaces). This second situation is the closest to the substrate used by Jimenez-Solomon et al.[20]

The combination of the effects mentioned would give rise to different polyamide thin layers. The outer surface, smoother and with smaller pores, has allowed the creation of a less permeable thin film, whereas the inner surface a more permeable thin film. In agreement with this and according to the C/N and the O/N obtained from the XPS, the inner PA layer is less cross-linked than the outer one (28.39 of C/N and 5.72 of

O/N in the inner PA compared to 6.81 of C/N and 2.07 O/N in the outer PA). These measurements support the hypothesis extracted from the Young-Laplace equation (Equation 6), which suggests that smaller superficial pores would lead to denser films, while larger pores give rise to more porous films. The density of the film is closely related to the cross-linking of the polymer, so it is reasonable to have less cross-linking degree in the inner PA thin film.

Finally, the synthesis procedure that leads to either the outer or the inner TFC could also influence the final PA thin film morphology. As other authors have mentioned, microfluidic synthesis possesses many advantages over traditional syntheses, such as high synthesis control (concentration and time), low radial concentration gradients and lack of turbulence (laminar flow).[16,17] These advantages are important to create homogenous and defect free TFC membranes.

TFC performance based on the mathematical model

The performance of two HF configurations was modelled: 1) PA on the inner side and 2) PA on the outer side of the fiber. The size of the mesh used in the simulation was chosen on the basis of computational cost and reproducibility of hydrodynamic results. On this regard, the computational domain was discretized by more than 157000 triangular elements defining a structured mesh, with an edge length in the range of 0.0016 to 0.09 cm in both cases, of PA on the inner and outer sides of the HF configuration. An "opening" boundary of the outlet was applied to both types of modelling, which means that the fiber was opened and there was no accumulation inside the channel. To be able to simulate the flux through a given membrane, it was crucial to define the model input that consist of inlet flow, species concentration, pressure, temperature, porosity and geometry of the HF (see values in Table 3 below).

Table 3. Summary of the main parameters used for the computer modelling.

Parameter	Symbol	Value	Units
Pressure	P	$8 \cdot 10^{5}$	Pa
Temperature	T	293.15	K
AO density	AO_{ρ}	1.015	$kg \cdot m^{-3}$
AO viscosity	AO_{μ}	$1.19 \cdot 10^{-5}$	Pa·s
Flow rate	V	$3 \cdot 10^{-9}$	$m^{3} \cdot s^{-1}$
Velocity on the walls	u	0	$m^{3} \cdot s^{-1}$

Inflow concentration	c_0	$56.6 \cdot 10^{-3}$	$mol \cdot m^{-3}$
HF inner diameter	d_{in}	250	µm
HF outer diameter	d_{out}	380	µm
Selective layer thickness, inner	t_{in}	50	nm
Selective layer thickness, outer	t_{out}	70	nm

The model output that can be extracted from the simulations consists of variety of different parameters such as flow velocity, pressure, flux, concentration, among others. Fig. S3A shows the hollow fiber configuration with PA on the outer layer (marked blue), Fig. S3B shows the pressure distribution along the fiber for the same configuration and Fig. S3C shows the total flux across the geometry. The same output results were extracted from the PA on the inner layer geometry (see Fig. 6A-C) which yielded the higher experimental permeance.

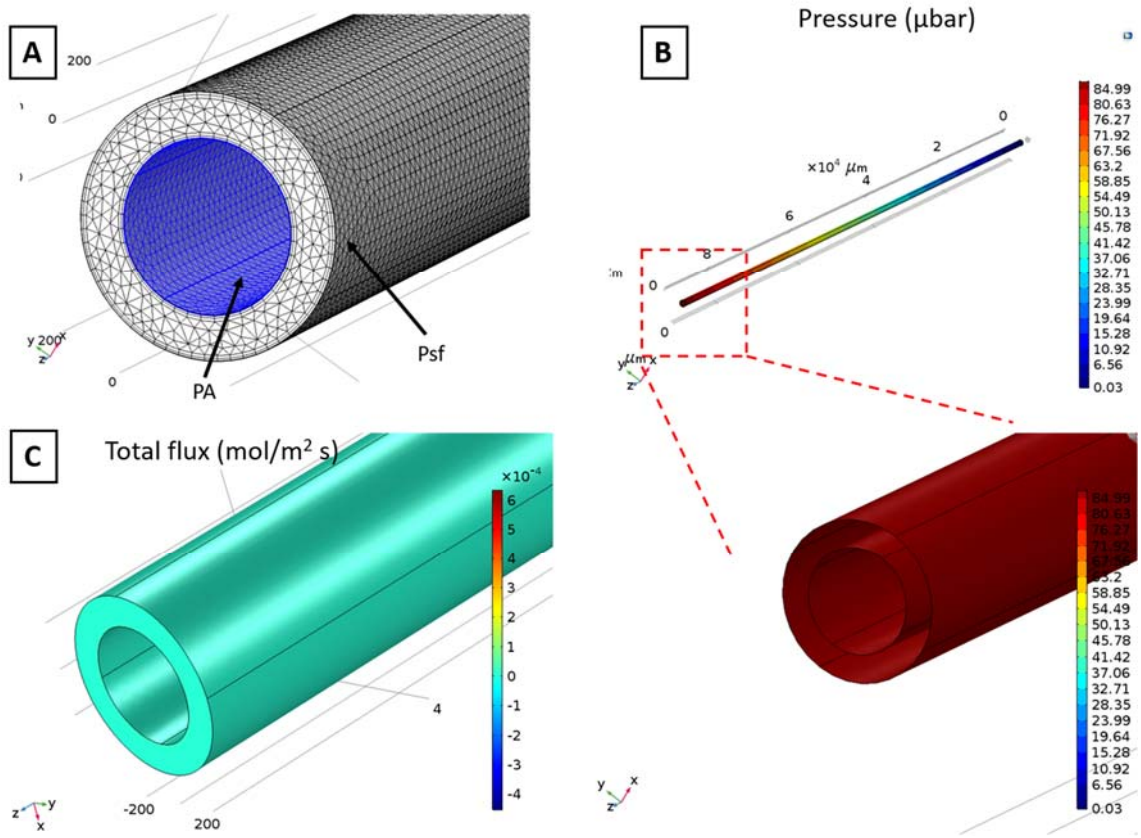

Fig. 6. Hollow fiber configuration with PA on the inner layer (A). Pressure distribution along the fiber (B). Total flux of AO across the fiber (C).

The final results were obtained by an integration of the inner/outer surface. The values extracted from COMSOL Multiphysics had to be recalculated in order to be able to compare them to the experimental results. In case of the inner configuration the mathematically modelled permeance is equal to 2.45 $L \cdot m^{-2} \cdot h^{-1} \cdot bar^{-1}$ while in the case of outer configuration the simulated permeance is equal to 0.31 $L \cdot m^{-2} \cdot h^{-1} \cdot bar^{-1}$. Both of them, are similar to the values obtained in the second hour of the nanofiltration experiments (Fig. 4B). It was observed that after 2 h of the experiment, the measurements stabilized and the permeance as well as rejection values began to be reproducible. Hence, it was decided to compare these values to the modelled ones (see Table 4). The slight differences between model and experiments can be related to either an experimental error or lack of the experimental data. Especially the values of the thickness of the selective layer in the inner HF configuration were difficult to estimate. Moreover, it is of crucial importance to bear in mind that the computer modelling always shows the so-called "ideal case scenario", where the experimental fluctuation of i.e. temperature, pressure, flow rate etc. are not considered. Nevertheless, it is confirmed both experimentally and mathematically, that the higher values of permeance were obtained in the case of the inner HF configuration. This is connected with lower thickness and surface area of the membrane.

Table 4. Experimental and simulated values comparison between permeance through the outer PA layer and the inner PA layer. Conditions: 20 ºC and 8 bar of feed pressure

Water permeance values	Experimental (t= 2 h)	Simulation
Through outer PA ($L \cdot m^{-2} \cdot h^{-1} \cdot bar^{-1}$)	0.19	0.31
Through inner PA ($L \cdot m^{-2} \cdot h^{-1} \cdot bar^{-1}$)	2.99	2.45

Comparison with other results in the literature

It is of interest to compare the results obtained in this work with others corresponding to TFC membranes for nanofiltration and reverse osmosis found in the literature. Both hollow fiber and flat membranes have been considered. The results and the references are shown in Fig. 7. Besides, Table S1 in the SI shows other relevant data about these membranes.

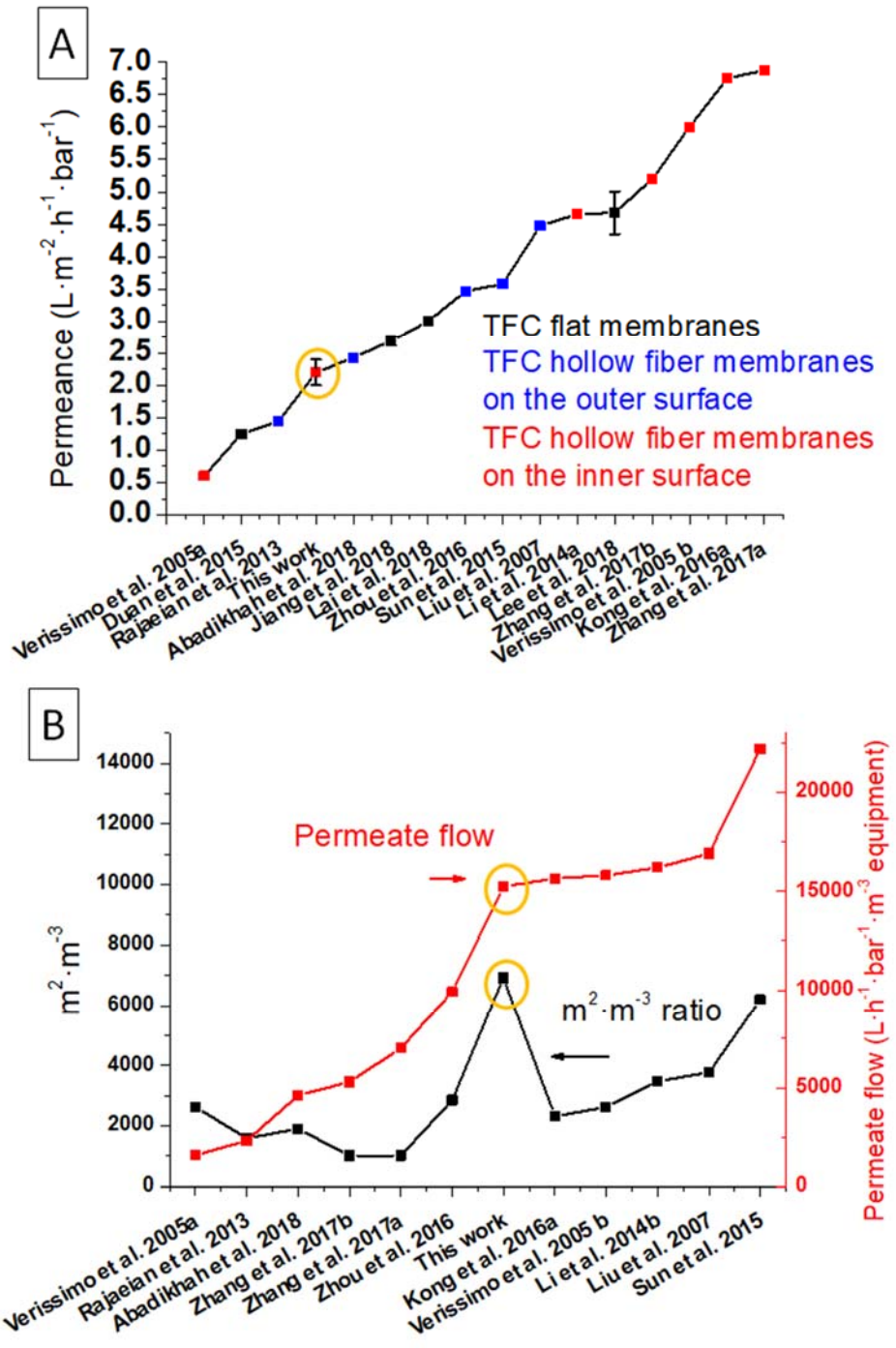

Fig. 7. Water permeance in RO and NF for different TFC membranes compared with the membrane fabricated in this work, highlighted with the orange circle (A). See further information about these membranes in Table S1.[10–13,21,26,31–39] *Comparison of m^2/m^3 ratio and permeate flow per bar and per m^3 of equipment between TFC membranes with the PA thin film formed on the lumen side from other works and the results of the present work, highlighted in orange circles (B). See further information about these membranes in Table S2 of SI.*[10–12,31,32,35–40]

Lee et al.[21] and Lai et al.[34] have recently studied the optimization of TFC membranes for reverse osmosis applications. Both of them found ways to maximise the permeance of water without decreasing the rejection values. In particular, Lee et al.[21] investigated the formation of highly porous microstructured substrates, obtaining mechanically stable narrow finger pores along the structure with about 40 nm of pore diameter. This result contrasts with the structure of the membrane fabricated in the present work, whose cross section had a rather symmetric pore size distribution along the diameter with inner pore diameters of about 2 – 3 μm. According to Lee et al.[21], the superficial porosity (size and hollow spaces distribution) influenced the PA formation. However, in the TEM images shown here (see Figs. 3E and 3F) it seems that the pore aperture influenced the MPD diffusion and hence the PA film morphology, as Ghosh and Hoek observed.[19]

Compared to the results obtained in the present work, Lee et al.[21] and Lai et al.[34] obtained higher values of water permeance (3 and 4.68 $L \cdot m^{-2} \cdot h^{-1} \cdot bar^{-1}$ respectively, compared to 2.2 $L \cdot m^{-2} \cdot h^{-1} \cdot bar^{-1}$, see Fig. 7A and Table S1). However, they used flat non-commercial supports. In contrast, the substrate in the current work was a commercial hollow fiber support, highly suitable for industrial implementation. Besides, as other authors have highlighted, the modules filled with hollow fibers have a higher membrane area/module volume ratio compared to those of flat membranes.[16,17]

Several authors achieved the fabrication of TFC membranes on polymeric hollow fibers leading to higher permeances than those obtained in the present work (in the 2.4-6.9 $L \cdot m^{-2} \cdot h^{-1} \cdot bar^{-1}$ range compared to 2.2 $L \cdot m^{-2} \cdot h^{-1} \cdot bar^{-1}$ achieved in this work, see Fig. 7A and Table S1).[11-13,32,35–39] Abadikhah et al.[32], Sun et al.[36], Liu et al.[37] and Zhou et al.[35] synthesized the polyamide thin layer on the outer surface of a non-commercial supports such as Si_3N_4/PES, Matrimid® dual-layer hollow fiber membrane, PVDF and PES, respectively (see Table S1). In contrast, Verissimo et al.[39], Kong et al.[11], Li et al.[13], Zhang et al.[12,38] fabricated TFC hollow fiber membranes with the selective layer on the inner surface. Among them, Verissimo et al.[39] did not fabricate a sufficiently selective membrane, since the rejection obtained was 77% for the sucralose (see Table S1). On the contrary, Kong et al.[11] and Li et al.[13] did fabricate highly selective TFC membranes (98% for $MgSO_4$ in both cases, see Table S1) using commercial PVC and polysulfone substrates, respectively. Finally, Zhang et al.[12,38] did not used commercial hollow fiber membranes in none of the referred publications, but they achieved selective membranes for nanofiltration and reverse osmosis applications (94.9% and 94.2 for sucrose and $MgCl_2$, respectively, see Table S1).

In terms of a hypothetical membrane module, most authors used hollow fibers with a wider inner and outer diameter than those used in the present work, which would lead to a less compactation.[10–13,31,32,35,37–39] Only Sun et al.[36] used hollow fibers with narrower inner and outer diameters (190 and 350 µm, respectively) in comparison to those used in this work (250 and 380 µm for inner and outer diameter respectively), which is an advantage, since this leads to a higher m^2/m^3 ratio. In fact, a membrane module with a volume of 1 m^3 built with the fibers used in our study would achieve a m^2/m^3 ratio of ca. 6890, while the rests would achieve a value significantly lower (see Fig. 7B and Table S2). This ratio has an influence on the total permeate flow, since it is taken into account in its calculation and, as Fig. 8B and Table S2 show, it compensates the relatively low permeances of the TFC membrane we synthesized. In fact, it is seen that, compared to other membranes, ours could compete in terms of permeate flow (15235, 15651, 15806, 16199, 16906 $L \cdot h^{-1}$ for the present work, Kong et al.[11], Verissimo et al.[39], Li et al.[13] and Liu et al.[37] respectively), even though the permeances were different (see Fig. 7A and Table S1). In contrast, Sun et al., would achieve a higher total flux (22211 $L \cdot h^{-1}$), but the substrate they used was tailor-made. In the rest of publications, the total flow would be lower due to a lower m^2/m^3 ratio.[10,12,31,32,35,38] Finally, Verissimo et al.[10], Duan et al.[26] and Rajaeian et al.[31] achieved the fabrication of membranes whose performances showed lower water permeances than that achieved in this work.

Conclusion

The influence of porosity and superficial roughness on the formation of the PA thin film of a TFC membrane was demonstrated. The large pores of the microfiltration hollow fiber substrates used here enabled the fabrication of TFC membranes with high water permeance. However, both the inner and outer surfaces of the hollow fibers had different pore sizes and roughness, which led to TFC membranes with different properties. The lumen side presented larger pores, with apertures of about 2700 nm. In contrast, the outer surface of the hollow fiber had a smoother surface with smaller pores of ca. 900 nm. The consequences for the TFC membrane performances were very important: the microfluidics helped to create a more stable membrane, which showed a constant permeance during five hours of selective nanofiltration. In addition, the PA layer polymerized on the support surfaces had different morphology: full PA-polysulfone contact was observed on the outside of the hollow fiber while a discontinuous PA-polysulfone contact occurred on the inside of the support, evidencing a lighter membrane structure. In consequence, the TFC membranes prepared on the inside of the hollow fiber supports were more permeable with higher rejection values than those fabricated on the outer side. These results were confirmed by a mathematical

simulation run with the COMSOL Multiphysics 5.3 software. The smaller pores on the outer surface of the support in contact with the PA film are more susceptible to fouling with dye (Acridine Orange) than the larger support pores on the inner surface in contact with the PA layer.

In addition to the high nanofiltration performance of the TFC membrane obtained in this work, this membrane has the advantage of being fabricated on a commercial hollow fiber substrate. Even if the fabricated membrane was apparently not the most permeable among those reported in the literature, here it is demonstrated how the higher surface to volume (m^2/m^3) ratio compared to other ratios found in the literature would enable a membrane module to be built with at least the same permeate flow per bar and per m^3 of equipment.

1. Acknowledgements

Financial support from the Spanish MINECO and FEDER (MAT2016-77290-R), the Aragón Government (T43-17R) and the ESF is gratefully acknowledged. C. Echaide-Górriz thanks the Aragón Government for his PhD grant. We also acknowledge Polymem for the hollow fiber supports. All the microscopy work was done in the Laboratorio de Microscopías Avanzadas at the Instituto de Nanociencia de Aragón (LMA-INA). The authors acknowledge the LMA-INA for offering access to their instruments and expertise.

2. Bibliography

1. Hermans S, Marien H, Van Goethem C, Vankelecom IFJ. Recent developments in thin film (nano)composite membranes for solvent resistant nanofiltration. *Curr. Opin. Chem. Eng.* 2015;8:45–54.
2. Vandezande P, Gevers LEM, Vankelecom IFJ. Solvent resistant nanofiltration: separating on a molecular level. *Chem. Soc. Rev*. 2008;37:365–405.
3. Jeong BH, Hoek EMV, Yan YS, Subramani A, Huang XF, Hurwitz G, Ghosh AK, Jawor A. Interfacial polymerization of thin film nanocomposites: A new concept for reverse osmosis membranes. *J. Membr. Sci.* 2007;294(1–2):1–7.
4. Vanherck K, Aerts A, Martens J, Vankelecom I. Hollow filler based mixed matrix membranes. *Chem. Commun.* 2010;46:2492–2494.
5. Peyravi M, Jahanshahi M, Rahimpour A, Javadi A, Hajavi S. Novel thin film nanocomposite membranes incorporated with functionalized TiO2 nanoparticles for organic solvent nanofiltration. *Chem. Eng. J*. 2014;241:155–166.
6. Roy S, Ntim SA, Mitra S, Sirkar KK. Facile fabrication of superior nanofiltration membranes from interfacially polymerized CNT-polymer composites. *J. Membr. Sci*. 2011;375:81–87.
7. Namvar-Mahboub M, Pakizeh M, Davari S. Preparation and characterization of UZM-5/polyamide thin film nanocomposite membrane for dewaxing solvent recovery. *J. Membr. Sci*. 2014;459:22–32.
8. Sorribas S, Gorgojo P, Tellez C, Coronas J, Livingston AG. High Flux Thin Film Nanocomposite Membranes Based on Metal-Organic Frameworks for Organic Solvent Nanofiltration. *J. Am. Chem. Soc*. 2013;135:15201–15208.

9. Parthasarathy A, Brumlik CJ, Martin CR, Collins GE. Interfacial polymerization of thin polymer-films onto the surface of a microporous hollow-fiber membrane. *J. Membr. Sci*. 1994;94:249–254.
10. Verissimo S, Peinemann KV, Bordado J. Thin-film composite hollow fiber membranes: An optimized manufacturing method. *J Membr. Sci*. 2005;264(1–2):48–55.
11. Kong X, Zhou MY, Lin CE, Wang J, Zhao B, Wei XZ, Zhu BK. Polyamide/PVC based composite hollow fiber nanofiltration membranes: Effect of substrate on properties and performance. *J. Membr. Sci*. 2016;505:231–240.
12. Zhang HZ, Xu ZL, Tang YJ, Ding H. Highly chlorine-tolerant performance of three-channel capillary nanofiltration membrane with inner skin layer. *J. Membr. Sci*. 2017;527:111–120.
13. Li HB, Wang W, Zhang YF. Preparation and Characterization of High-Selectivity Hollow Fiber Composite Nanofiltration Membrane by Two-Way Coating Technique. *J Appl. Polym. Sci*. 2014;131(23):11.
14. Kong X, Zhang Y, Zeng SY, Zhu BK, Zhu LP, Fang LF, Matsuyama H. Incorporating hyperbranched polyester into cross-linked polyamide layer to enhance both permeability and selectivity of nanofiltration membrane. *J. Membr. Sci*. 2016;518:141–149.
15. Kong X, Qiu ZL, Lin CE, Song YZ, Zhu BK, Zhu LP, Wei XZ. High permselectivity hyperbranched polyester/polyamide ultrathin films with nanoscale heterogeneity. *J. Mater. Chem. A*. 2017;5:7876–7884.
16. Echaide-Gorriz C, Clement C, Cacho-Bailo F, Tellez C, Coronas J. New strategies based on microfluidics for the synthesis of metal-organic frameworks and their membranes. *J. Mater. Chem. A*. 2018;6:5485–5506.
17. Elvira KS, Solvas XCI, Wootton RCR, deMello AJ. The past, present and potential for microfluidic reactor technology in chemical synthesis. *Nat. Chem*. 2013;5:905–915.
18. Shi L, Chou SR, Wang R, Fang WX, Tang CY, Fane AG. Effect of substrate structure on the performance of thin-film composite forward osmosis hollow fiber membranes. *J. Membr. Sci*. 2011;382:116–123.
19. Ghosh AK, Hoek EMV. Impacts of support membrane structure and chemistry on polyamide-polysulfone interfacial composite membranes. *J. Membr. Sci*. 2009;336:140–148.
20. Solomon MFJ, Gorgojo P, Munoz-Ibanez M, Livingston AG. Beneath the surface: Influence of supports on thin film composite membranes by interfacial polymerization for organic solvent nanofiltration. *J. Membr. Sci*. 2013;448:102–113.
21. Lee J, Wang R, Bae TH. High-performance reverse osmosis membranes fabricated on highly porous microstructured supports. *Desalination*. 2018;436:48–55.
22. Ren J, Chowdhury MR, Qi J, Xia LL, Huey BD, McCutcheon JR. Relating osmotic performance of thin film composite hollow fiber membranes to support layer surface pore size. *J. Membr. Sci*. 2017;540:344–353.
23. Echaide-Górriz C, Sorribas S, Téllez C, Coronas J. MOF nanoparticles of MIL-68(Al), MIL-101(Cr) and ZIF-11 for thin film nanocomposite organic solvent nanofiltration membranes. *RSC Adv*. 2016;6:90417–90426.
24. Echaide-Gorriz C, Navarro M, Tellez C, Coronas J. Simultaneous use of MOFs MIL-101(Cr) and ZIF-11 in thin film nanocomposite membranes for organic solvent nanofiltration. *Dalton Trans*. 2017;46:6244–6252.
25. Chai GY, Krantz WB. Formation and characterization of polyamide membranes via interfacial polymerization. *J. Membr. Sci*. 1994;93:175–192.
26. Duan JT, Pan YC, Pacheco F, Litwiller E, Lai ZP, Pinnau I. High-performance polyamide thin-film-nanocomposite reverse osmosis membranes containing hydrophobic zeolitic imidazolate framework-8. *J. Membr. Sci*. 2015;476:303–310.
27. Lin L, Feng C, Lopez R, Coronell O. Identifying facile and accurate methods to measure the thickness of the active layers of thin-film composite membranes – A comparison of seven characterization techniques. *J. Membr. Sci*. 2016;498:167–179.
28. Hansen CM. *Hansen Solubility Parameters: A User's Handbook*. Boca Raton: CRC Press, 2007.
29. Xie Q, Zhang S, Hong Z, Ma H, Liu C, Shao W. Effects of casting solvents on the morphologies, properties, and performance of polysulfone supports and the resultant graphene

oxide-embedded thin-film nanocomposite nanofiltration membranes. *Ind. Eng. Chem. Res*. 2018;57:16464–16475.
30. Razmjou A, Mansouri J, Chen V. The effects of mechanical and chemical modification of TiO_2 nanoparticles on the surface chemistry, structure and fouling performance of PES ultrafiltration membranes. *J. Membr. Sci*. 2011;378:73–84.
31. Rajaeian B, Rahimpour A, Tade MO, Liu SM. Fabrication and characterization of polyamide thin film nanocomposite (TFN) nanofiltration membrane impregnated with TiO_2 nanoparticles. *Desalination*. 2013;313:176–188.
32. Abadikhah H, Kalali EN, Behzadi S, Khan SA, Xu X, Agathopoulos S. Amino functionalized silica nanoparticles incorporated thin film nanocomposite membrane with suppressed aggregation and high desalination performance. *Polymer*. 2018;154:200–209.
33. Jiang ZW, Karan S, Livingston AG. Water transport through ultrathin polyamide nanofilms used for reverse osmosis. *Adv. Mater.* 2018;30:1705973.
34. Lai GS, Lau WJ, Goh PS, Ismail AF, Tan YH, Chong CY, Krause-Rehberg R, Awad S. Tailor-made thin film nanocomposite membrane incorporated with graphene oxide using novel interfacial polymerization technique for enhanced water separation. *Chem. Eng. J*. 2018;344:524–534.
35. Zhou BW, Zhang HZ, Xu ZL, Tang YJ. Interfacial polymerization on PES hollow fiber membranes using mixed diamines for nanofiltration removal of salts containing oxyanions and ferric ions. *Desalination*. 2016;394:176–184.
36. Sun SP, Chan SY, Chung TS. A slow-fast phase separation (SFPS) process to fabricate dual-layer hollow fiber substrates for thin-film composite (TFC) organic solvent nanofiltration (OSN) membranes. *Chem. Eng. Sci*. 2015;129:232–242.
37. Liu JQ, Xu ZL, Li XH, Zhang Y, Zhou Y, Wang ZX, Wang XJ. An improved process to prepare high separation performance PA/PVDF hollow fiber composite nanofiltration membranes. *Sep. Purif. Technol*. 2007;58:53–60.
38. Zhang HZ, Xu ZL, Ding H, Tang YJ. Positively charged capillary nanofiltration membrane with high rejection for Mg^{2+} and Ca^{2+} and good separation for Mg^{2+} and Li^{+}. *Desalination*. 2017;420:158–166.
39. Verissimo S, Peinemann KV, Bordado J. New composite hollow fiber membrane for nanofiltration. *Desalination*. 2005;184:1–11.
40. Li WB, Yang ZH, Zhang GL, Fan Z, Meng Q, Shen C, Gao CJ. Stiff metal-organic framework-polyacrylonitrile hollow fiber composite membranes with high gas permeability. *J. Mater. Chem. A.* 2014;2:2110–2118.

List of figures

Fig. 7. Water permeance in RO and NF for different TFC membranes compared with the membrane fabricated in this work, highlighted with the orange circle (A). See further information about these membranes in Table S1.[10–13,21,26,31–39] *Comparison of* m^2/m^3 *ratio and permeate flow per bar and per* m^3 *of equipment between TFC membranes with the PA thin film formed on the lumen side from other works and the results of the present work, highlighted in orange circles (B). See further information about these membranes in Table S2 of SI.*[10–12,31,32,35–40]